NUMERICAL STUDY OF INCOMPRESSIBLE FLOW AND HEAT TRANSFER IN NON-CIRCULAR DUCTS WITH CUSP CORNERS

Ass. Prof. Dr. Abdulkarim A. Hassan
Energy and Fuel Research Centre
University of Technology
Baghdad - Iraq

Qassim K. Hunaehn
Mechanical Engineering Department
University of Baghdad
Baghdad - Iraq

ABSTRACT

A numerical finite-volume calculation method was used for application to fully-developed flow and heat transfer in straight ducts with 2-Cusp, 3-Cusp and 4-Cusp cross-sectional area. The method was formulated with reference to a non-orthogonal curvilinear coordinate system which was fitted exactly into duct shape. In turbulent flow, the Reynolds stresses were calculated by using the coupled algebraic stress model of Launder and Ying (1973) with a ($k-\varepsilon$) transport model. This turbulent stress model enabled secondary flows to be included in the non-circular duct calculations. In heat transfer solution, three thermal boundary conditions were investigated.Predictions were compared with available numerical and experimental data. The turbulent flow predictions of secondary and axial velocity, wall shear stress and Nusselt number were in reasonable agreement with experiment for the fully-developed flow cases. It is concluded that, although the maximum secondary flow was found to be (1.5%-2.5%) of the mean axial flow, the absence of this flows have significant influence on the flow and heat transfer parameters. Moreover, these flows will increase when the corners of a duct become more acute. Heat transfer results showed that the peripheral temperature variation around the duct has a significant effect on the heat transfer results, and confirmed the inadequacy of the hydraulic radius concept in the cases of the very non-circular ducts when comparison is made with Blasius correlation.

الخلاصة

دراسة عددية باستخدام طريقة الحجوم المحددة تم تطبيقها لحساب الجريان وانتقال الحرارة في أنابيب ذات مقطع غير دائري وتحتوي على زوايا مستدقة.الدراسة اعتمدت على نظام المحاور الغير متعامدة والذي يأخذ شكل مقطع الأنبوب. في الجريان المضطرب, تم حساب اجهادات رينولدز باستخدام نموذج Launder and Ying (1973) مع نموذج $(k-\varepsilon)$, هذا النموذج قادر على حساب الجريان الثانوي الذي يتولد في الأنابيب الغير دائرية المقطع. في حساب انتقال الحرارة, ثلاثة شروط حدية تم تطبيقها. النتائج المستحصلة تم مقارنتها مع نتائج نظرية ومختبرية سابقة. نتائج الجريان المضطرب للسرعة الثانوية والمحورية واجهاد القص ورقم نسلت كانت مطابقة بشكل مقبول مع النتائج المختبرية المتوفرة. لقد تم الاستنتاج أنه رغم ان القيمة القصوى للجريان الثانوي تصل الى(1.5%-2.5%) من معدل الجريان المحوري ,الا أن تأثيره على النتائج واضح, فضلا عن أن هذا الجريان تزداد قوته مع وجود زوايا حادة في مقطع الأنبوب. نتائج أنتقال الحرارة أظهرت أن التغيير المحيطي لدرجة الحرارة حول الأنبوب له تأثير واضح على هذه النتائج وكذلك تبين ضعف مفهوم القطر المكافئ في حالة الانابيب ذوات الزوايا المستدقة عند المقارنة مع علاقة بلسيوس للانبوب الدائري المقطع.

KEYWORDS
non-circular ducts, cusp corners, turbulent flow, secondary flows

INTRUDUCTION

The need for compact flow passages in heat exchangers and other engineering component systems, like, the cooling and heating process in nuclear reactors and all kinds of waste-heat recovery have led to an urgent need for detailed knowledge of flow and heat transfer in non-circular ducts; in particle ducts with cusp corners. Such geometries, i.e. cusp corners, may be found in many applications like tube bundles and the shell and tube which form many types of heat exchangers. Therefore the study of these geometries, for both the flow and heat transfer, is very important in the industrial. This study will provide the require data for behavior of average and local properties for the flow and heat transfer like the friction resistance and the heat transfer coefficient.

For its mathematical simplicity, the fully-developed laminar flow in non-circular ducts has been solved for most practical geometries to investigate the effect of shape on the friction factor by using the hydraulic diameter concept. Examples of these investigations are the work of **(Gunn and Darling 1963)** as they carried out numerical study on fluid energy losses in non-circular conduits, especially sections formed by close packed tube bundles and they also investigated these shapes experimentally. **(Shah and London 1978)** showed that solutions of the governing differential equations have been obtained by both analytical and numerical methods for many non-circular geometries. It was found that non-circular ducts friction factor is always different from that of circular duct. The main reason for this difference is the deformation of the local wall shear stress, which is caused by the duct shape deformation.

A feature of turbulent flow in non-circular ducts which is absent from laminar flow is the "secondary flows" that are generated in the cross-sectional plane. These flows have the effect of transporting some of the core fluid into the corners of the duct, causing the flow to spiral in the axial direction in separate cells located across the cross-section. Although the secondary velocities are relatively weak compared with the main axial flow (about 1%-2.5% of mean axial velocity), but can have significant influence on the flow and heat transfer characteristics. Indeed, the distortions caused to the axial velocity distribution were the main early evidence of the existence of these flows in non-circular ducts.

Experimental work on turbulent flow in non-circular duct geometry is mainly confined to friction factor measurements. Examples of those are, **(Launder and Ying 1973)** for square duct, (Hassan 1984) for isosceles right angle triangular and 4-cusp ducts and **(Rijab et al 1991)** for 3-cusp duct. Previous experimental works showed that any prediction procedure must therefore include secondary flow effects if it is to produce realistic results. An alternative simplified approach was however taken by **(Launder and Ying 1973)** who developed approximate algebraic versions of the Reynolds stress transport equations for the calculation of square duct flow. These were later generalized by **(Gesener and Emery 1976)** who derived an algebraic equation set for the full Reynolds stress tensor. The prediction method of **(Launder and Ying 1973)** has been applied to the axial flow in equilateral triangular and square ducts **(Rapley 1980)**; isosceles right angle triangular and 4-cusp ducts **(Hassan 1984)** and trapezoidal and a wavy ducts **(Rokni and Gatski 1999).**

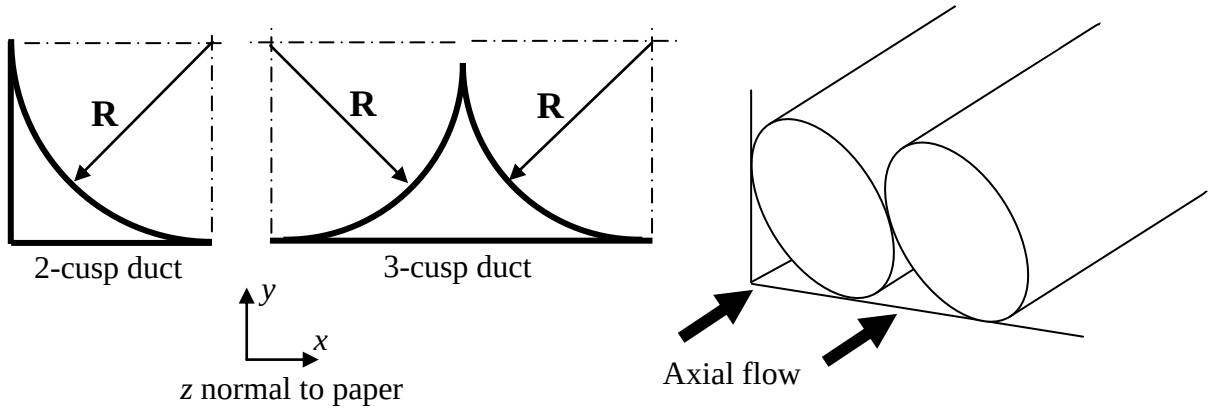

Fig.1: Ducts under consideration

The ducts shown in **Fig.1** are of particular interest because it represents the limiting case of compact rod bundle flows with rods touching with flat plates. Closely spaced rod bundles have important applications in nuclear reactor cores and other compact heat exchangers and, over the years, much effort has gone into methods of prediction **(Hassan 1984)**. However, no calculations of turbulent flow with predicted secondary flow appear to be available for 2-cusp and 3-cusp geometries. Such ducts yield a very non-circular passage shape with curved walls and cusped corners and are thus suitable for the present study. This should provide useful information on local mean flow, secondary flow and turbulence distributions and the problems associated with their prediction generally in this class of duct as well as specifically for the limiting case of rods touching in rod bundle flow.

In the present study, a numerical finite-volume procedure, used for the prediction of fully-developed turbulent flow in straight passages of arbitrary constant cross-section, is applied to 2-cusp and 3-cusp ducts, as shown in **Fig.1**. The method solves the Reynolds, continuity and turbulence transport equations on a non-orthogonal curvilinear grid which is generated numerically to fit the duct cross-section. The Reynolds stresses are calculated with an algebraic stress transport model (ASTM) of **(Launder and Ying 1973)** which links the stresses to mean velocity gradients through the turbulence kinetic energy and its dissipation rate, whose values are obtained by solving their modeled transport equations; i.e. (k-ε) model.

THEORETICAL MODEL

Governing Equations

The Reynolds equation for steady time-averaged incompressible turbulent flow can be written in Cartesian tensor form as **(Hinze 1975):**

$$\frac{\partial(\rho u_i u_j)}{\partial x_i} = -\frac{\partial P}{\partial x_j} + \frac{\partial(\sigma_{ij})}{\partial x_i} \tag{1}$$

and the continuity equation as:

$$\frac{\partial(\rho u_i)}{\partial x_i} = 0 \tag{2}$$

The stress tensor σ_{ij} represents the sum of the viscous and turbulent (Reynolds) stresses, i.e.

$$\sigma_{ij} = \mu\left(\frac{\partial u_i}{\partial x_j} + \frac{\partial u_j}{\partial x_i}\right) - \rho\,\overline{u_i' u_j'} \tag{3}$$

And the energy equation:

$$\frac{\partial}{\partial x_j}\left(\rho u_j T\right) = \frac{\partial}{\partial x_j}\left[\frac{\mu}{\Pr}\frac{\partial T}{\partial x_j}\right] + \frac{\partial}{\partial x_j}\left(-\overline{\rho u_j' t}\right) \tag{4}$$

The terms ($\overline{\rho u_j' t}$) represent the *turbulent heat fluxes.* Simply eddy diffusivity (SED) model based on the Boussinesq approximation is used to provide closure these fluxes, **(Rokni and Gatski 1999).**

$$\overline{\rho u_j' t} = -\frac{\mu_t}{\sigma_T}\frac{\partial T}{\partial x_i} \tag{5}$$

substituting **eq.(5)** into **eq.(4)** gives:

$$\frac{\partial}{\partial x_j}\left(\rho u_j T\right) = \frac{\partial}{\partial x_j}\left[\left(\frac{\mu}{\Pr} + \frac{\mu_t}{\sigma_T}\right)\frac{\partial T}{\partial x_j}\right] \tag{6}$$

Turbulence Modeling

As attention previously, generation of secondary flows by numerical model is an important factor to accurately the prediction of turbulent flow in non-circular passages. A linear eddy-viscosity model (EVM) does not have the ability to predict secondary flows, this being a consequence of the stresses being directly related to co-planar velocity gradients, as with fully-developed laminar flow. This means that a higher order turbulent stress model is needed, which usually entails solving the Reynolds stress transport equations for each stress required. Therefore, the algebraic stress transport model (ASTM) of **(Launder and Ying 1973)** is used in the present study to describe the Reynolds stresses, as:

$$\overline{w'w'} = C_1 k \tag{7}$$

$$\overline{v'v'} = C_3 k - C_2 C_4\left(\frac{k^3}{\varepsilon^2}\right)\left(\frac{\partial w}{\partial y}\right)^2 \tag{8}$$

$$\overline{u'u'} = C_3 k - C_2 C_4\left(\frac{k^3}{\varepsilon^2}\right)\left(\frac{\partial w}{\partial x}\right)^2 \tag{9}$$

$$\overline{u'v'} = \overline{v'u'} = -C_2 C_4\left(\frac{k^3}{\varepsilon^2}\right)\left(\frac{\partial w}{\partial x}\right)\left(\frac{\partial w}{\partial y}\right) \tag{10}$$

$$\overline{u'w'} = -C_4\left(\frac{k^2}{\varepsilon}\right)\left(\frac{\partial w}{\partial x}\right) \tag{11}$$

$$\overline{v'w'} = -C_4\left(\frac{k^2}{\varepsilon}\right)\left(\frac{\partial w}{\partial y}\right) \tag{12}$$

In order to be consistent with the aim of obtaining a prediction procedure for general geometries, no attempt has been made to optimize the empirical constant, whose values have simply been taken from previous studies, **(Launder and Ying 1973)** and **(Rapely 1980)** and may be summaries below:

C_1=0.23,C_2=0.027,C_3=0.562 and C_4=C_μ =0.09

The axial plane shear stresses $\overline{\rho u'w'}$ and $\overline{\rho v'w'}$ are seen from **eq.(11)** and **eq.(12)** to be represented by a gradient diffusion model with an isotropic turbulent viscosity μ_t given by **(Jones and Launder(1972)**:

$$\mu_t = C_\mu \rho \frac{k^2}{\varepsilon} \tag{13}$$

In contrast the cross-plane stresses, which are responsible for secondary flows, are seen from **eqs.(8)-(10)** to depend on strain rates in planes normal to the cross-plane.

The turbulence quantities k and ε, required in the ASTM, were obtained here from the appropriate from of the well-known (k-ε) two equation turbulence model **(Launder and Spalding 1974):**

$$\frac{\partial}{\partial x_j}\left(\rho u_j k\right) = \frac{\partial}{\partial x_j}\left[\left(\mu + \frac{\mu_t}{\sigma_k}\right)\frac{\partial k}{\partial x_j}\right] + G \ - \rho\varepsilon \tag{14}$$

$$\frac{\partial}{\partial x_j}\left(\rho u_j \varepsilon\right) = \frac{\partial}{\partial x_j}\left[\left(\mu + \frac{\mu_t}{\sigma_\varepsilon}\right)\frac{\partial \varepsilon}{\partial x_j}\right] + \frac{\varepsilon}{k}\left(C_{\varepsilon 1} G \ - C_{\varepsilon 2}\rho\varepsilon\right) \tag{15}$$

Where σ_k=1.0 and σ_ε=1.2 are the turbulent Prandtl numbers for k andε, respectively, $C_{\varepsilon 1}$=1.55, $C_{\varepsilon 2}$=2.0 and G is the generation rate of turbulence kinetic energy, calculated from **(Hassan 1984);**

$$G \cong \frac{\mu_t}{\rho}\left[\left(\frac{\partial w}{\partial x}\right)^2 + \left(\frac{\partial w}{\partial y}\right)^2\right] \tag{16}$$

Transformation of the Governing Equations

The governing equations can be written in terms of a single general equation for an arbitrary scalar dependent variable as

$$\frac{\partial}{\partial x_j}\left(\rho u_j \phi\right) = \frac{\partial}{\partial x_j}\left[\Gamma\left(\frac{\partial \phi}{\partial x_j}\right)\right] + S_\phi \tag{17}$$

where Γ is an effective diffusion coefficient and S_ϕ is a source term. **Eq.(17)** when cast into general non-orthogonal form with, the aid of the transformation of **(Rhie 1985)** to new independent variables ($\zeta,,\eta$) and specialized to fully-developed flow in straight passages ($\partial/\partial z$ =0 except $\partial P/\partial z$ and $\partial T/\partial z$ **(Kays and Crawford 1993)**), **eqs.(1),(2),(6),(14)** and **(15)** can be written:

u - Momentum: $$\frac{\partial(\rho G_1 u)}{\partial\zeta}+\frac{\partial(\rho G_2 u)}{\partial\eta}=\frac{\partial}{\partial\zeta}\left(\frac{\mu}{J}\alpha\frac{\partial u}{\partial\zeta}\right)+\frac{\partial}{\partial\eta}\left(\frac{\mu}{J}\gamma\frac{\partial u}{\partial\eta}\right)+S_{MX} \quad (18)$$

v - Momentum: $$\frac{\partial(\rho G_1 v)}{\partial\zeta}+\frac{\partial(\rho G_2 v)}{\partial\eta}=\frac{\partial}{\partial\zeta}\left(\frac{\mu}{J}\alpha\frac{\partial v}{\partial\zeta}\right)+\frac{\partial}{\partial\eta}\left(\frac{\mu}{J}\gamma\frac{\partial v}{\partial\eta}\right)+S_{MY} \quad (19)$$

w - Momentum: $$\frac{\partial(\rho G_1 w)}{\partial\zeta}+\frac{\partial(\rho G_2 w)}{\partial\eta}=\frac{\partial}{\partial\zeta}\left(\frac{\mu}{J}\alpha\frac{\partial w}{\partial\zeta}\right)+\frac{\partial}{\partial\eta}\left(\frac{\mu}{J}\gamma\frac{\partial w}{\partial\eta}\right)+S_{MZ} \quad (20)$$

Continuity Equation: $$\frac{\partial(\rho G_1)}{\partial\zeta}+\frac{\partial(\rho G_2)}{\partial\eta}=0 \quad (21)$$

Energy eq.: $$\frac{\partial(\rho G_1 T)}{\partial\zeta}+\frac{\partial(\rho G_2 T)}{\partial\eta}=\frac{\partial}{\partial\zeta}\left[\left(\frac{\mu}{\Pr}+\frac{\mu_t}{\sigma_T}\right)\frac{\alpha}{J}\frac{\partial T}{\partial\zeta}\right]+\frac{\partial}{\partial\eta}\left[\left(\frac{\mu}{\Pr}+\frac{\mu_t}{\sigma_T}\right)\frac{\gamma}{J}\frac{\partial T}{\partial\eta}\right]+S_T \quad (22)$$

k-Equation: $$\frac{\partial(\rho G_1 k)}{\partial\zeta}+\frac{\partial(\rho G_2 k)}{\partial\eta}=\frac{\partial}{\partial\zeta}\left[\left(\mu+\frac{\mu_t}{\sigma_k}\right)\frac{\alpha}{J}\frac{\partial k}{\partial\zeta}\right]+\frac{\partial}{\partial\eta}\left[\left(\mu+\frac{\mu_t}{\sigma_k}\right)\frac{\gamma}{J}\frac{\partial k}{\partial\eta}\right]+S_k \quad (23)$$

ε-Equation: $$\frac{\partial(\rho G_1 \varepsilon)}{\partial\zeta}+\frac{\partial(\rho G_2 \varepsilon)}{\partial\eta}=\frac{\partial}{\partial\zeta}\left[\left(\mu+\frac{\mu_t}{\sigma_\varepsilon}\right)\frac{\alpha}{J}\frac{\partial\varepsilon}{\partial\zeta}\right]+\frac{\partial}{\partial\eta}\left[\left(\mu+\frac{\mu_t}{\sigma_\varepsilon}\right)\frac{\gamma}{J}\frac{\partial\varepsilon}{\partial\eta}\right]+S_\varepsilon$$

(24)

here G_1 and G_2 are contravariant velocities:

$$\left.\begin{aligned} G_1 &= u\frac{\partial y}{\partial\eta}-v\frac{\partial x}{\partial\eta}\\ G_2 &= v\frac{\partial x}{\partial\zeta}-u\frac{\partial y}{\partial\zeta}\end{aligned}\right\} \quad (25)$$

Where J,α,β and γ can be found in **(Karki and Patankar 1989)**. Details of the source term S_ϕ for each equation can be found in **Table 1**. The turbulent stresses appearing in these source terms were calculated with the ASTM **eqs.(8)-(12).**

Table 1: Parameters in the General Transport Equation.

Equation	ϕ	S_ϕ
Continuity	1	0
x-Momentum	u	$-\frac{\partial P}{\partial x}-\frac{\partial}{\partial x}\left(\overline{\rho u'u'}\right)-\frac{\partial}{\partial y}\left(\overline{\rho v'u'}\right)-\frac{\partial}{\partial z}\left(\overline{\rho w'u'}\right)$
y-Momentum	v	$-\frac{\partial P}{\partial y}-\frac{\partial}{\partial x}\left(\overline{\rho u'v'}\right)-\frac{\partial}{\partial y}\left(\overline{\rho v'v'}\right)-\frac{\partial}{\partial z}\left(\overline{\rho w'v'}\right)$
z-Momentum	w	$-\frac{\partial P}{\partial z}-\frac{\partial}{\partial x}\left(\overline{\rho u'w'}\right)-\frac{\partial}{\partial y}\left(\overline{\rho v'w'}\right)-\frac{\partial}{\partial z}\left(\overline{\rho w'w'}\right)$
Energy	T	$\rho w J\frac{\partial T}{\partial z}$
Turbulent energy	k	$-\rho\varepsilon+G$

Turbulent dissipation	ε	$\frac{\varepsilon}{k}(C_1 G - C_2 \rho \varepsilon)$

Boundary Conditions

The treatment of solid wall boundaries includes the most difficult part of solving the problem of flow and heat transfer in non-circular duct. The boundary conditions applied around the duct periphery involved the use of wall functions to bridge between the interior solution and wall surfaces. The functions used were conventional and based on the well-known "log-law of the wall" which is written **(Versteeg and Malalasekera 1995)**;

For momentum: $$\frac{U}{u_\tau} = \frac{1}{\kappa}\ln(E Y^+) \tag{26}$$

where *U* represents the local resultant velocity and

$$Y^+ = \frac{\rho u_\tau y_n}{\mu} \tag{27}$$

with y_n the distance from the wall along the appropriate coordinate line. u_τ is the local friction velocity taken here as

$$u_\tau = \tau_w / \rho C_\mu^{1/4} k^{1/2} \tag{28}$$

with τ_w the local wall shear stress, κ=0.42 and *E*=9.025 as in **(Rapley 1980).**

The above relations were used to obtain local wall shear stress for solution of the momentum equations and together with the assumption of local turbulence equilibrium also to obtain relations for the near-wall generation and dissipation of turbulence kinetic energy for solution of the turbulence equations **(Rapley 1980)**.

For energy: $$T^+ = \sigma_T \left[U^+ + f(\sigma_L/\sigma_T)\right] \tag{29}$$

where T^+ is a non-dimensional temperature defined by**(Versteeg and Malalasekera 1995)**:

$$T^+ = \frac{\rho u_\tau c_P}{q_w}(T_w - T_P) \tag{30}$$

where T_w is the wall temperature, T_P is the near wall temperature and q_w is the wall heat flux.

and $$f(\sigma_L/\sigma_T) = 9.24\left[\left(\frac{\sigma_L}{\sigma_T}\right)^{0.75} - 1\right] \times \left\{1 + 0.28\exp\left[-0.007\frac{\sigma_L}{\sigma_T}\right]\right\} \tag{31}$$

as well as, three thermal boundary conditions are applied for heat transfer field as in **(Rapley 1980)**
H1: Constant peripheral temperature and axial heat flux.
H2: Constant peripheral and axial temperature (isothermal wall).
H3: Constant peripheral and axial heat flux.

THE NUMERICAL SOLUTION

The transport equations, i.e. **eq.(18), eq.(19)** and **eq.(20)** for momentum, **eq.(22)** for energy and **eq.(23)** and **eq.(24)** for turbulence, can all be cast into the following common form:

$$\frac{\partial}{\partial\zeta}(\rho\phi G_1)+\frac{\partial}{\partial\eta}(\rho\phi G_2)+\frac{\partial}{\partial z}(\rho\phi G_3)=\frac{\partial}{\partial\zeta}\left(\frac{\Gamma_\phi}{J}\alpha\frac{\partial\phi}{\partial\zeta}\right)+\frac{\partial}{\partial\eta}\left(\frac{\Gamma_\phi}{J}\gamma\frac{\partial\phi}{\partial\eta}\right)+\frac{\partial}{\partial z}\left(J\Gamma_\phi\frac{\partial\phi}{\partial z}\right)+S_{Total} \quad (32)$$

Where ϕ stands for any of the main dependent variables *u, v, w, T, k* and ε . Γ_ϕ and S_{Total} are respectively the corresponding diffusion term and source, where $S_{Total}=S_N+JS_\phi$, and S_N is the source term arising from the nonorthogonality of the grid system,

$$S_N=-\left[\frac{\partial}{\partial\eta}\left(\frac{\Gamma_\phi}{J}\beta\frac{\partial\phi}{\partial\zeta}\right)+\frac{\partial}{\partial\zeta}\left(\frac{\Gamma_\phi}{J}\beta\frac{\partial\phi}{\partial\eta}\right)\right] \quad (33)$$

and the details of the appropriate Γ_ϕ and S_ϕ for each equation can be found in **Table 1**.

A finite-volume method was used, based on a non-orthogonal grid in the duct cross-plane, **Fig. 2**, and employing a staggered grid arrangement for *u* and *v* **(Versteeg and Malalasekera 1995)**.

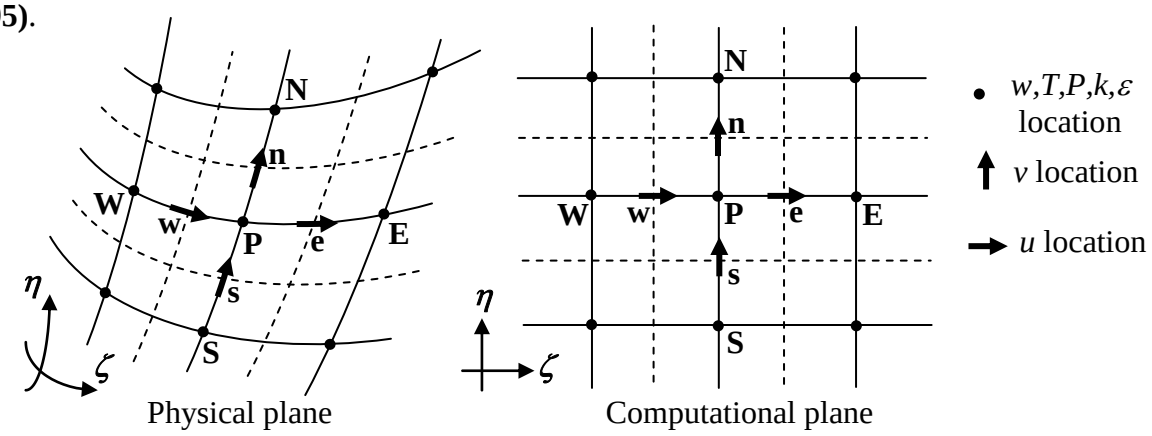

Fig. 2: The cross-plane non-orthogonal curvilinear grid

Integration of each term in **eq. (32)** across the appropriate control volumes led to the final discretized algebraic equation, i.e.

$$(A_P - S_P)\phi_P = A_E\phi_E + A_W\phi_W + A_N\phi_N + A_S\phi_S + S_C \tag{34}$$

where $A_P = A_E + A_W + A_N + A_S$ and S_P and S_C are coefficients of the linearized sources. The A coefficients contain the combined effects of convection and diffusion approximated by a standard hybrid differencing scheme **(Patankar 1980)**. The solution procedure consisted of a repeated outer sequence in which the cross-plane momentum and continuity equations were dealt with by the SIMPLE method of **(Patankar 1980),** and an inner iteration sequence in which the discretized algebraic equations were solved with a conventional line-by-line method based on the well known tri-diagonal matrix algorithm (TDMA). Because of the inherent non-linearity of the discretization equation it is sometimes necessary to slow down the change in ϕ from one iteration to the next, so in the present study, under-relaxation used to avoid divergence to the solution **(Rapley 1980)**. The convergence requirement used was that the sum of the absolute residual sources over the whole field be less than 10^{-3} of reference quantities based on overall mass and momentum flows.

RESULTS AND DISSCUSION

Grid Generation

The non-orthogonal body-fitted curvilinear grid used in the flow and heat transfer predications for 2-Cusp and 3-Cusp ducts was generated numerically by using the most common elliptic partial differential equation, Laplace equation, in the form:

$$\left.\begin{aligned}\frac{\partial^2\zeta}{\partial x^2} + \frac{\partial^2\zeta}{\partial y^2} = 0\\ \frac{\partial^2\eta}{\partial x^2} + \frac{\partial^2\eta}{\partial y^2} = 0\end{aligned}\right\} \tag{35}$$

The above were solved by finite differences using central differencing and a similar ADI algorithm to that used in the flow solution. Typical full mesh generated for the present cases shown in **Fig. 3** and **Fig. 4**. Tests with different meshes were used to obtain mean flow solutions that were substantially independent of the mesh and as may be expected, the secondary flow field was found to be more sensitive to mesh changes than mean flow particularly in the regions where nodes became sparse.

The Flow and Heat Transfer Calculations

At first of these calculations, the flow was assumed to be unidirectional flow (without secondary flows). The unidirectional solution severed a number of purposes. The primary purpose was to set it as a first estimate to the solution when the full flow problem is considered. This was found to be very effective in enhancing the stability and convergence rate of the numerical solution. Moreover, the results of the unidirectional solution for the ducts under consideration are compared with these with secondary flow to see the effect of secondary flows on the various parameters. The unidirectional flow is considerably simpler than that with secondary flow, since the mathematical problem is reduced to a one-dimensional problem. It is necessary to solve the axial momentum equation with the $(k-\varepsilon)$ turbulence model. The results of this flow will be shown and discussed along with the other results in the following section.

For 2-Cusp duct, the flow in this geometry must represent one of the more severe tests of the present calculation method, particularly in the absence of the smaller acute angle, where the axial velocity, turbulence properties and stresses change rapidly across the narrow duct. A further physical feature of this flow should be the significant damping effect of the walls on turbulence in the acute-angled corner. **Fig. 5** shows the axial velocity plotted at side bisector. The difference between the prediction for unidirectional flow and the real situation is attributed to the influence of the direction of rotation of the secondary flow which caused a reduction of the axial velocity in the side bisector. The effect of Reynolds number on the axial velocity is shown also and as expected, as the flow rate increases the velocity field becomes more full. The predicted secondary velocity vectors in the whole duct geometry are shown in **Fig. 6**. In the symmetry half of the duct, three swirls of secondary flow are predicted with two counter-rotating cells near the acute angle and the other near the right angle. Although there are no theoretical or experimental data available for comparison, the overall pattern seems a logical extrapolation of the isosceles right angle triangular duct flow pattern of **(Hassan 1984)**, and contains the usual features of flow from the core region along corner bisectors into the corners, then returning to the core via the walls and their perpendiculars. The largest secondary velocities are about 1.2% of the mean axial velocity and occur along the corner bisectors and base wall. The effect of secondary flows on the axial velocity contours can be seen in **Fig. 7**.

The predicted wall shearing stress along the curved side and the flat side is plotted in **Fig. 8.** The effect of flow rate and secondary flows is apparent on the distribution of the wall shear stress along the two walls of the duct, and it is similar to that in the axial velocity. The effect of secondary flow in reducing the peripheral variation is evident with reduced shear stress as approach to the center wall. This tendency of secondary flow to make wall shear more uniform is apparent in all previous non-circular passages studied **(Rapley 1980)** and **(Rokni and Gatski 1999)** and can be considered a further characteristic effect of secondary flow on the mean flow.

In heat transfer calculations, the heat transfer was obtained for three thermal boundary conditions, H1, H2 and H3. Details of the treatment of these boundary conditions can be found in **(Rapley 1980).** Air was chosen as a working fluid in these calculations and its properties were taken at bulk temperature of the flow field as in **(Kays and Crawford 1993)**. The local distribution of the heat transfer coefficient for the three boundary conditions, H1, H2 and H3 is presented in **Fig. 9**. The heat transfer coefficient in the case of H3 boundary condition varies steeply in the peripheral direction when compared with that for the other two boundary conditions H1 and H2. This behaviour of the heat transfer coefficient is strongly related to the distribution of the wall temperature in the peripheral direction. The effect of flow rate is presented in **Fig. 9**; therefore as the flow rate increases the profile of the heat transfer coefficient becomes more full. However, the variation of the heat transfer coefficient with the flow rate is very slight for the range of Reynolds numbers in the figure. The effect of the secondary flow is also evident in **Fig. 10** and it is similar to that observed on the local wall shear stress. Therefore, the secondary flow acts to increase the heat transfer coefficient in the corner region and at the same time reduces it in the central region. The mean Nusselt number-Reynolds number characteristics are shown in **Fig. 11**. The relation between the three thermal boundary conditions confirms the previous conclusions from the distributions of heat transfer coefficient. As expected, the predicted results for H1 and H2 are (40%) and (50%) respectively below the pipe flow correlation, whereas the H3 line is about (87%) lower than that of the pipe flow. Moreover, the uniform wall temperature (H1) boundary condition has the maximum value of mean Nusselt number whereas the uniform heat flux case, (H3) is always the smallest. This is caused by the presence of the transverse temperature gradient which is accompanying the H3 boundary condition and does not exist in the H1 boundary condition.

In 3-Cusp duct, **Fig. 12** shows the predicted axial velocity at two sections, the corner and side bisectors; a comparison between the present predictions and experimental data of (Rijab et al 1991), is also made. It is clear that the agreement along the side bisector is very good. Moreover,

the effect of secondary flow is clear also as it tends to make the axial velocity more full near the corner and reduces it near the side bisector. The predicted secondary velocity vectors in the 3-Cusp duct are shown in **Fig. 13**. Although, there is no experimental or theoretical pattern available with which to compare the latter, the three eddies obtained in the symmetry cell are consistent with the equilateral triangular duct case of **(Rapley 1980)** and **(Rokni and Gatski 1999)**, in that flow is from the core region towards the corner along the line of the corner bisecting plane, returning via the walls and wall bisecting planes. The largest secondary velocities were about 1.5% of the mean axial velocity and were located near the wall and along the corner bisector. The axial velocity contours which are presented in **Fig. 14** shows clearly the effect of the secondary flow in convecting the momentum from high momentum central regions towards the low momentum corner regions.

In **Fig. 15** the predicted local wall shear stress is compared with the measurements that made by (Rijab et al 1991). Several indications can be drawn from this figure which confirms those observed earlier in the axial velocity predictions. It is clear that the shear stress decreases near the corners, with higher gradient near the smaller angle. This is due to the laminarization of the flow near the corners. The decrease near the center of the flat is attributed to the existence of the secondary flow, as the secondary flow tends to make wall shear stress more uniform along the section and this similar to the results of **(Hassan 1984)**, in isosceles right angle triangle.

The present calculations for the local distribution of heat transfer coefficient are compared with the experimental measurements of (Rijab et al 1991). The experimental duct had electrically heated walls which were assumed to produce a constant heat flux, H3, boundary condition. This comparison is shown in **Fig. 16** where the present prediction is seen to be in reasonable overall agreement with experiment. The local distribution of heat transfer coefficient for the three boundary conditions H1, H2 and H3 is presented in **Fig. 17**. The present calculations show, however, that the peripheral variation of the heat transfer coefficient in the case of H3 is very steep compared with that of H1 and H2. The main reason is the steep variation of the temperature field in the peripheral direction. The significant effect of secondary flow in making the peripheral variation more uniform is evident from these results. The mean heat transfer coefficient is shown in Nusselt number form in **Fig. 18**. It is apparent from this figure that the difference between H1 and H2 Nusselt number is small. This is expected since the peripheral temperature variations are quite small. On the other hand, the mean Nusselt number for H2 and H3 cases is about 5% and 65% respectively below that of H1; this is caused by the severe wall temperature variations in the peripheral direction in H3 boundary condition.

CONCLUSIONS:

A numerical solution was developed for solving the flow and heat transfer fields in 2-Cusp and 3-Cusp ducts. In flow field, the flow was assumed to be hydrodynamically and thermally fully-developed flow. The secondary flows calculated by using ASTM of **(Launder and Ying1973)**. In heat transfer field, three thermal boundary conditions, H1, H2 and H3 were investigated. The results of the present study were in good agreement with the previous measurements. The following conclusions are indicated from the predictions:

1. In turbulent flow, it is evident that the two-equations ($k-\varepsilon$) model is quite a satisfactory model for turbulent flow in non-circular ducts.

2. The predicted axial velocity and wall shear stress distributions obtained for turbulent flow in corresponding ducts studied were generally found to be flatter than might be expected from the equivalent laminar calculations, taking into account the increased shear due to turbulence. The reason for this was clearly revealed by taking advantage of the facility in the present method of being able to make calculations for the hypothetical situation in which the turbulence secondary flow is suppressed.

3. The algebraic stress transport model (ASTM) of **(Launder and Ying 1973)** have the ability, rather than eddy-viscosity turbulence models, to predicate the secondary flow in straight non-circular ducts.

4. The secondary flows so generated, will distort the mean flow since axial velocity gradients, turbulence kinetic energy and wall shear stress will tend to increase in regions where secondary flow is directed towards the wall, and decrease in regions where it is directed away from the wall. This effect will be seen in axial velocity contours which will bulge into a wall convergence, and in wall shear stresses which will be made more evenly distributed.

5. In turbulent heat transfer, the effect the secondary flow on the local temperature distributions and local heat transfer coefficient was found to be quite significant which indicates the importance of including the secondary flow in the calculations.

REFERENCES

Gunn, D.J. and Darling, M.D. (1963), Fluid Flow and Energy Losses in Non-circular Conduits, Trans. Inst. Chem. Engrs., Vol. 41, pp. 163.

Hassan, A.K.A. (1984), Forced Convection in Isosceles Right Angle Triangular and 4-Cusp Ducts, Ph. D. Thesis, University of Liverpool, U.K.

Hinze, J.O. (1975), Turbulence, McGraw-Hill, New York.

Jones, W.P. and Launder, B.E. (1972), The Prediction of Laminarization with a Two-equation Model of Turbulence, Int. J. Heat Mass Transfers, Vol. 15, pp. 301.

Karki, K. and Patankar, S. (1989), Pressure Based Calculation Procedure for Viscous Flows at All Speeds in Arbitrary Configurations, AIAA Journal, Vol.27, pp. 1167-1174.

Kays, W.M. and Crawford, M.E. (1993), Convective Heat and Mass Transfer, 3rd edition, McGraw-Hill, New York.

Launder, B.E. and Spalding, D.B. (1974), The Numerical Computational of Turbulent Flow, Computer Methods in Applied Mechanics and Engineering, Vol.3, pp. 269-289.

Launder, B.E. and Ying, W.M. (1973), Prediction of Flow and Heat Transfer in Ducts of Square-Section, Proc. I. Mech. E., Vol. 187, pp. 455.

Patankar, S.V. (1980), Numerical Heat Transfer and Fluid Flow, Hemisphere, McGraw-Hill, New York.

Patankar, S.V. and Spalding, D.B. (1972), A Calculation Procedure for Heat Mass and Momentum Transfer in 3D Parabolic Flows, Int. J. Heat Transfer, Vol.15, pp. 1785.

Rapely, C. W. (1980), Fluid and Heat Flow in Tubes of Arbitrary Cross-Section, Ph.D. Thesis, University of London, U.K.

Rhie, C. M. (1985), A Three-Dimensional Passage Flow Analysis Method Aimed at Centrifugal Impellers, Computers and Fluids, Vol. 13, No. 4, pp. 443-460

Rijab, M.S., Hassan, A.K.A. and Muhsen, S.A. (1991), Turbulent Fluid Flow in Three-Cusp Duct,

مجلة الهندسة والتكنولوجيا, المجلد العاشر – العدد السادس (الملحق) ص109.

Rokni, M. and Gatski, T.B. (1999), Predicting Turbulent Convective Heat Transfer in Three-Dimensional Duct Flows, NASA/TM-1999-209843.

Shah, R.K. and London, A.L. (1978), Laminar Flow Forced Convection in Ducts, Advances in Heat Transfer, Academic Press, New York.

Versteeg, H.K. and Malalasekera, W. (1995), An Introduction to Computational Fluid Dynamics, the Finite Volume Method, Longman Scientific and Technical.

NOMENCLATURE

Latin Symbols

A: Coefficient of the discretized equations
C_1, C_2, C_3, C_4: Constants in ASTM
cp : Specific heat at constant pressure , J/(kg.K)
$C_\mu, C_{\varepsilon 1}, C_{\varepsilon 2}$: Constants in ($k-\varepsilon$) turbulence model
D : Diffusion term
E : Logarithmic law constant, equation (3.58)
F : Convection term
g : Metrics tensor element
G : Generation term of the turbulent kinetic energy
$G1, G2, G3$: Contravariant velocity components
h : Heat transfer coefficient, W/(m^2.K)
J : Jacobian of transformation
k : Turbulence kinetic energy, m^2/s^2
Nu : Nusselt number
P : Pressure, N/m^2
q'' : Heat flux, W/m^2
Re : Reynolds number
S_ϕ : Source term of ϕ ,table (3-1)
S_N : Source term due to non-orthogonality, equation (3.40)
S_{Total} : Total source terms
T : Temperature, K
T_b : Bulk (mixed) fluid temperature, K
u, v, w : Cartesian velocity components, m/s
x, y, z : Cartesian coordinate, m
U^+ : Dimensionless velocity, eq. 3.54)
Y^+ : Dimensionless distance from a wall, equation(3.52)

Greek Symbols

α, β, γ : Coordinate transformation parameters, equation(3.29)
δ_{ij} : Kronecker delta
Δ : Grid spacing, m
λ : Under-relaxation factor
ΔV : Elementary volume, m^3
Γ : Diffusion coefficient
ε : Dissipation rate of kinetic energy, N/(s.m^2)
κ : Von Karman constant
μ : Laminar viscosity, kg/(m.s)
μ_e : Effective total viscosity,($\mu+\mu_t$), kg/(m.s)
μ_t : Turbulent viscosity, kg/(m.s)
ν : Kinematics viscosity, m^2/s
ζ, η: Curvilinear coordinates
ρ : Density, kg/m^3
σ_{ij} : Stress tensor, N/m^2
$\sigma_k, \sigma_\varepsilon$: Effective Prandtl numbers
τ_{ij} : Viscous stress tensor, N/m^2

τ_w :Wall shear stress, N/m^2

ϕ :Dependent variable

Subscripts

e,w,n,s :Face of the control volume
E,W,N,S :Neighbor nodes of point p
i,j :Index Notations or coordinate direction identifiers
L :Local value
m :Mean value
MX,MY,MZ :Refers to source term of momentum equation in Cartesian coordinates
nb :Abbreviation of neighboring

Superscripts

* :Guessed quantity or quantity from last iteration
′ :Fluctuating quantity in the time averaging or correction quantity
— :Averaged quantity

Abbreviations

ASTM :Algebraic stress transport model
CFD :Computational Fluid Dynamics
SIMPLE :Semi- Implicit Method for Pressure Linked Equation
TDMA :Tridiagonal Matrix Algorithm

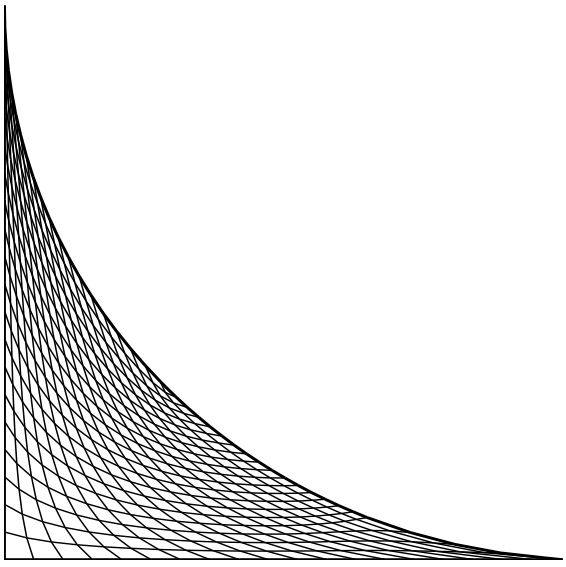

Fig.3: Non-orthogonal curvilinear grid for 2-cusp duct

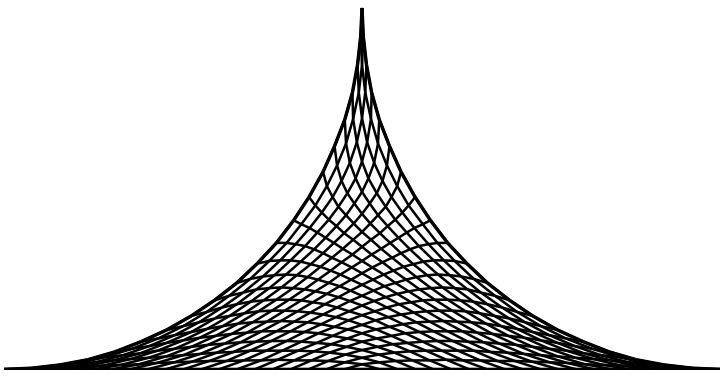

Fig.4: Non-orthogonal curvilinear grid for 3-cusp duct

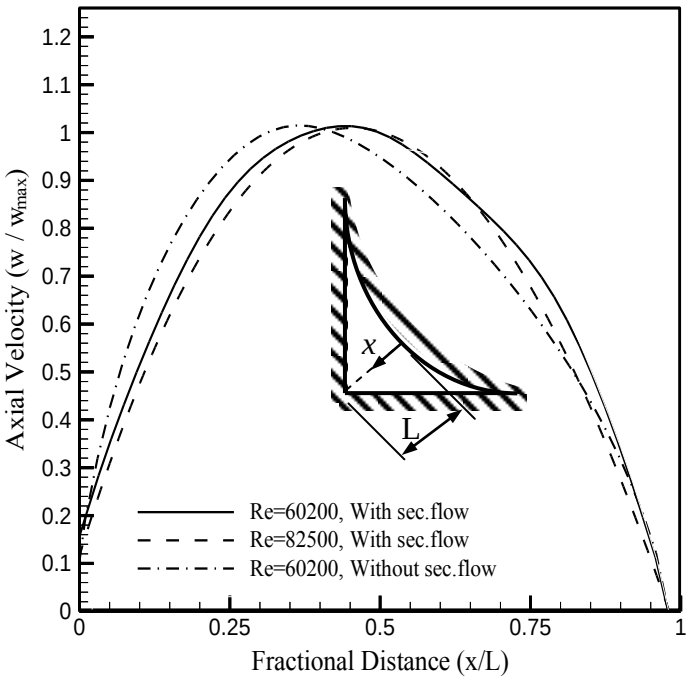

Fig.5: Axial velocity prediction in 2-cusp duct.

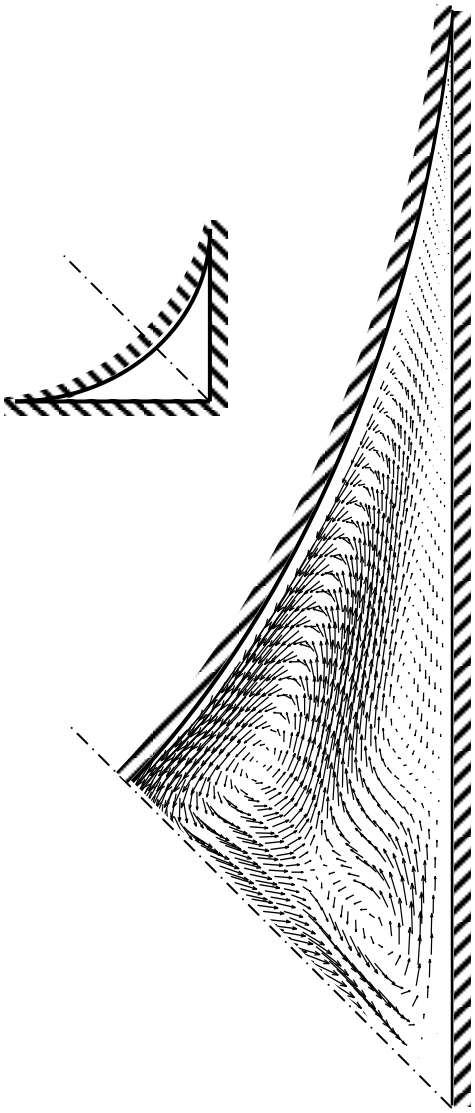

Fig.6: Predicted secondary velocity vectors in 2-cusp duct, Re=60200

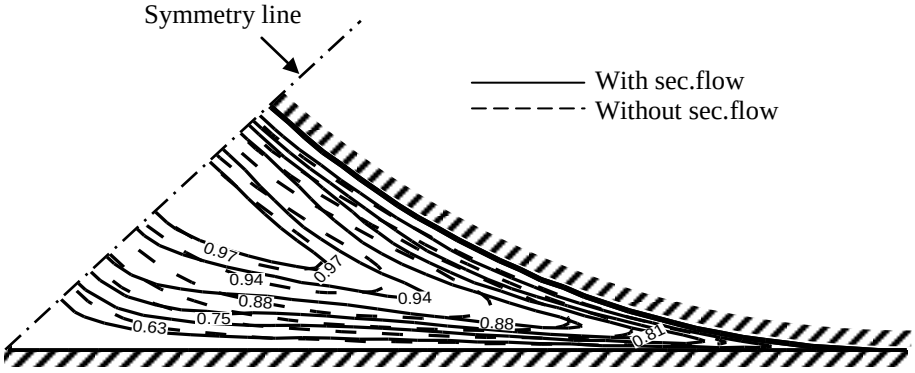

Fig.7: Axial velocity contours in turbulent flow in the 2-cusp duct, Re=60200

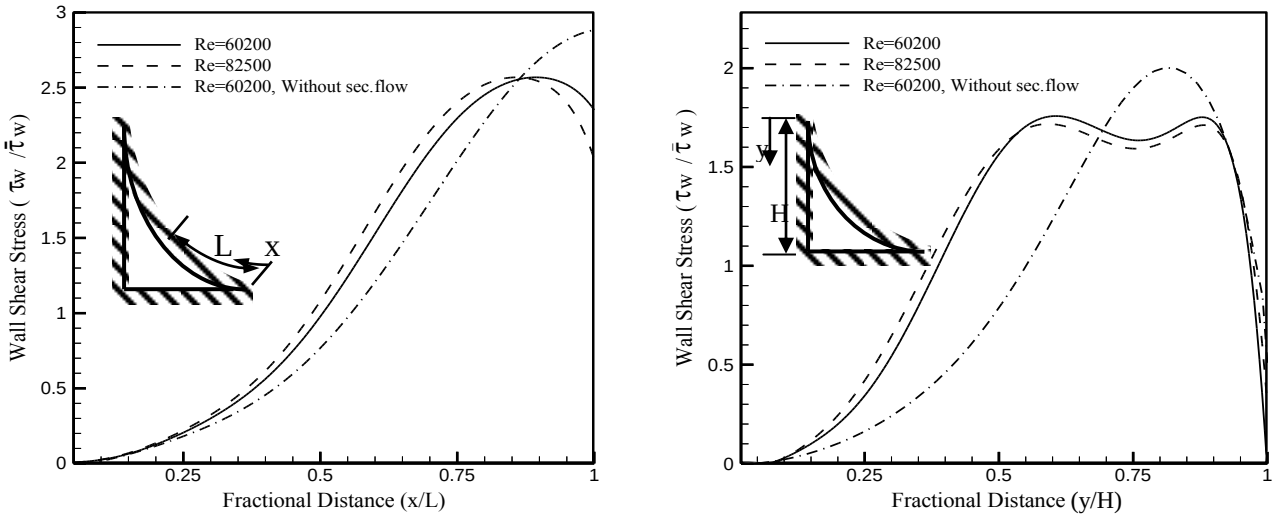

Fig.8: Wall shear stress prediction in turbulent flow in 2-cusp duct

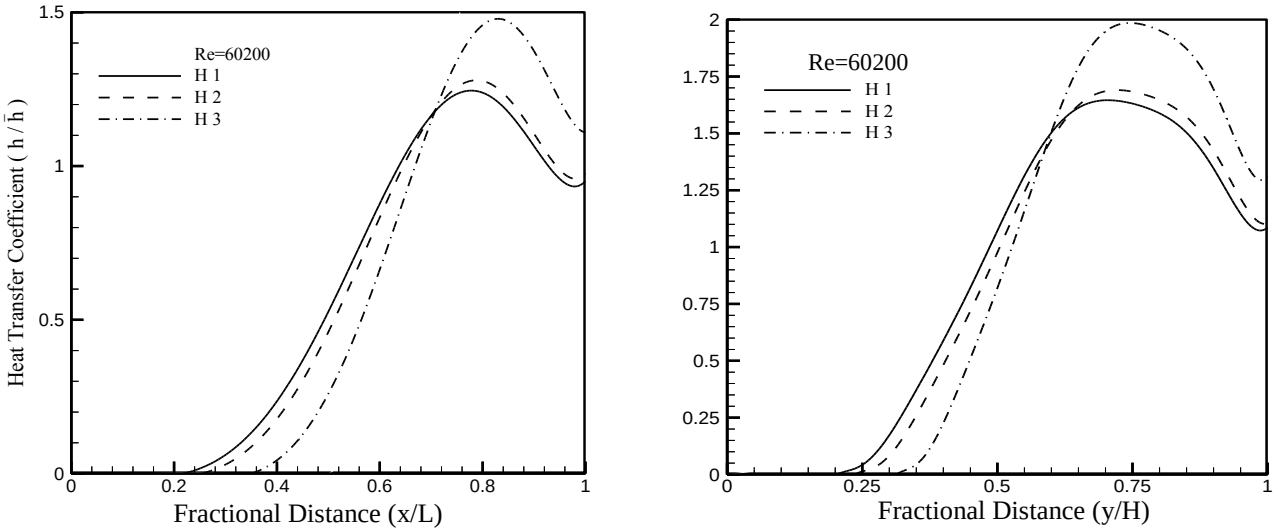

Fig.9: Predicted local distribution of heat transfer coefficient in 2-Cusp duct
(Effect of thermal boundary conditions)

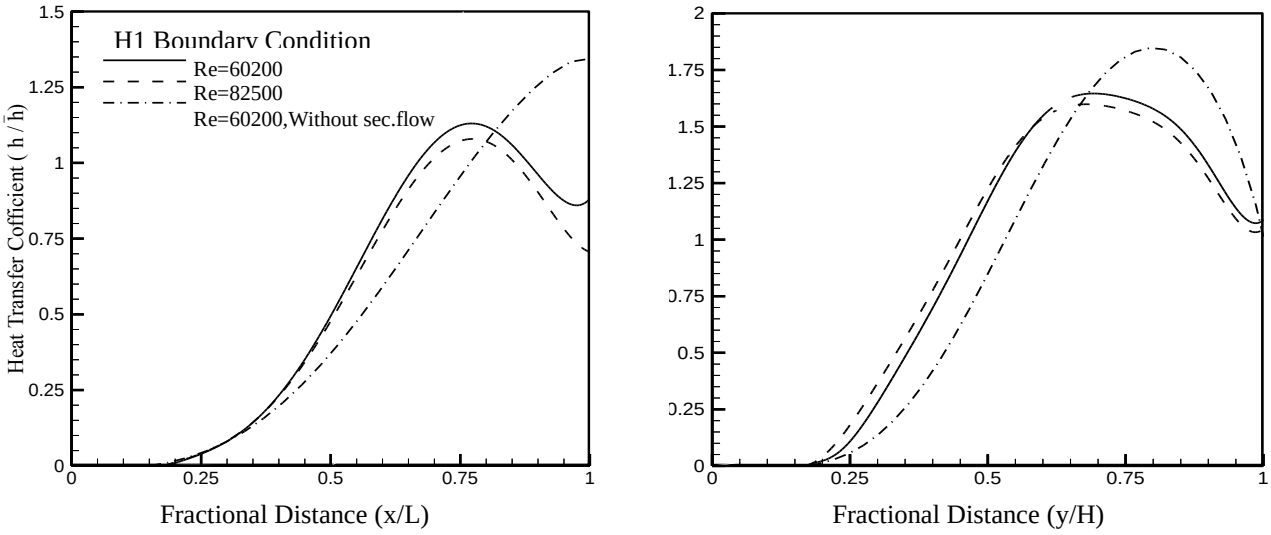

Fig.10: Predicted local distribution of heat transfer coefficient in 2-Cusp duct
(Effect of the secondary flow and the flow rate)

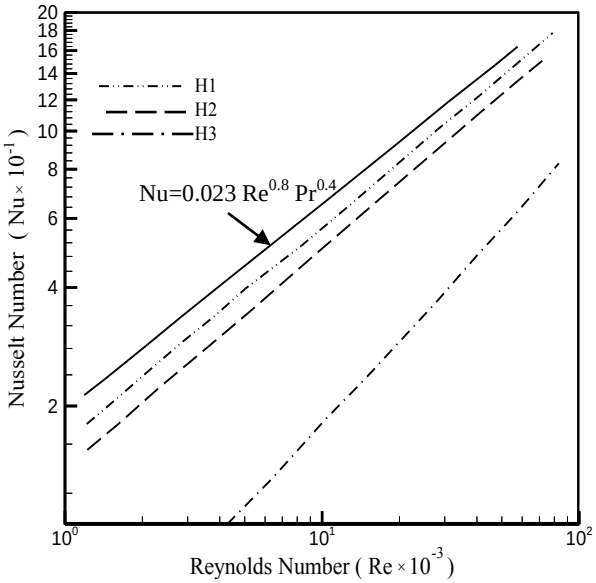

Fig.11: Predicted Nusselt number in 2-cusp Duct.

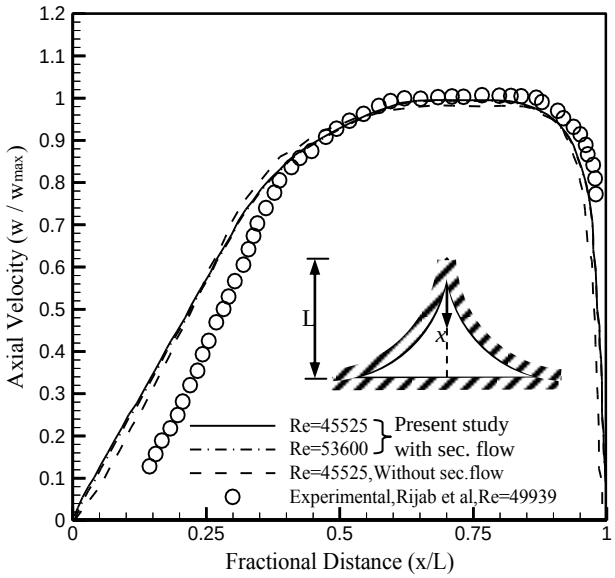

Fig.12-a: Axial velocity in turbulent Flow in 3-cusp duct (corner bisector)

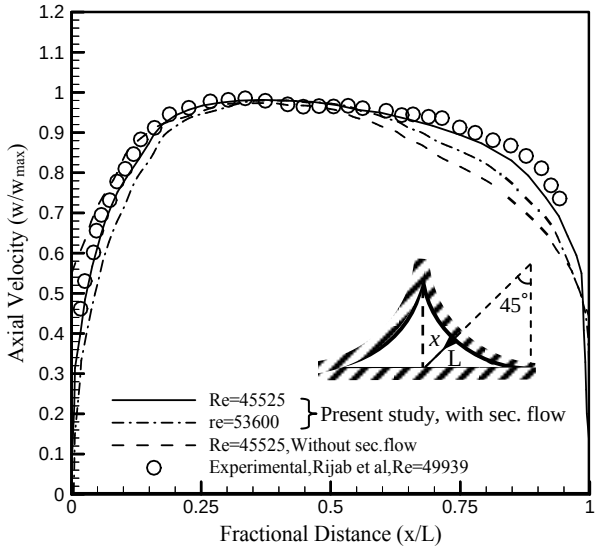

Fig.12-b: Axial velocity in turbulent flow in 3-cusp duct (side bisector)

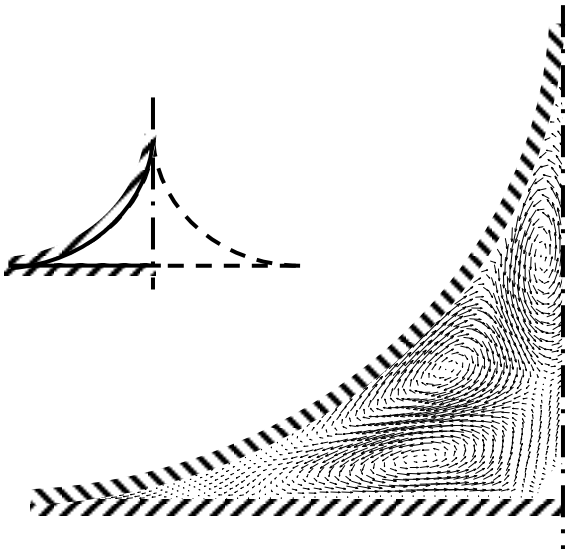

Fig.13: Predicted secondary velocity vectors in 3-cusp duct, Re=45525

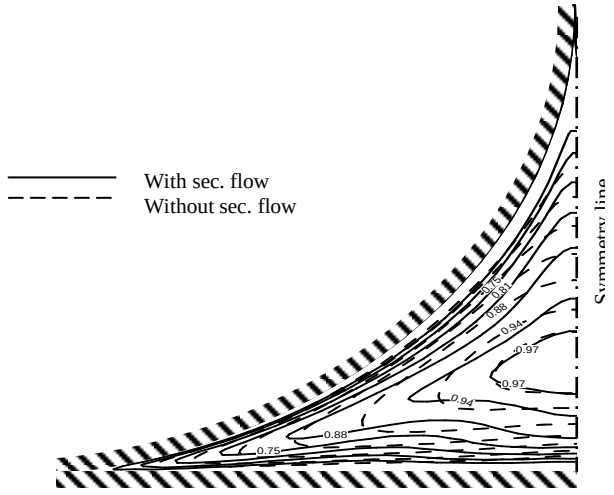

Fig.14: Axial velocity contours in turbulent flow in the 3-cusp duct, Re=45525

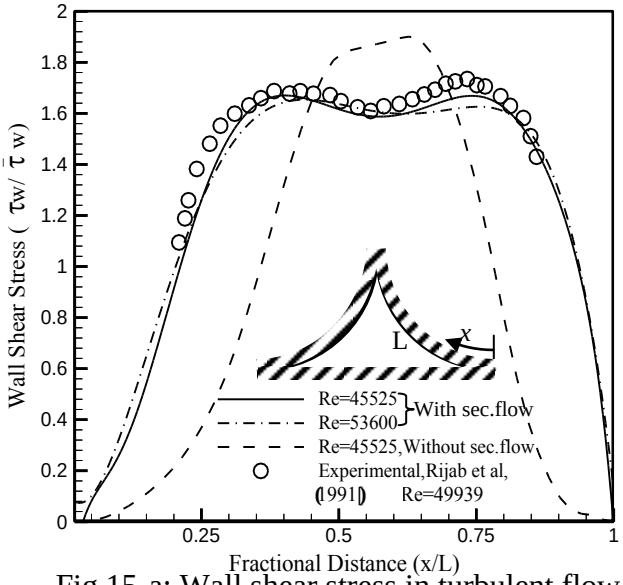

Fig.15-a: Wall shear stress in turbulent flow in 3-cusp duct.

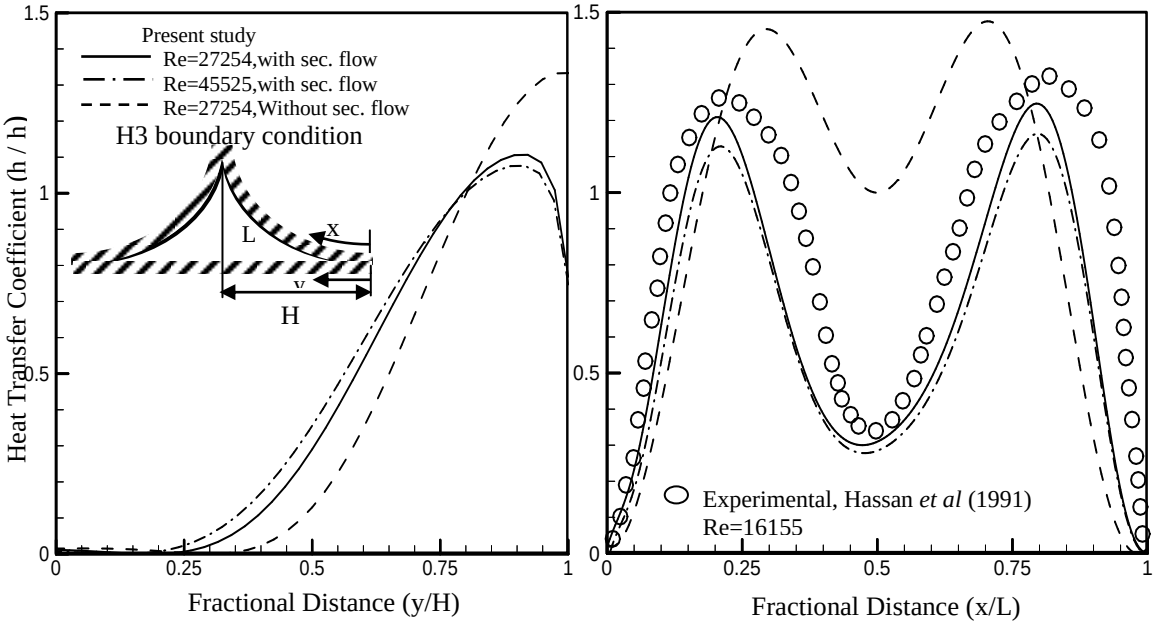

Fig.16: Effect of the secondary flow and the flow rate on the distribution of heat transfer coefficient

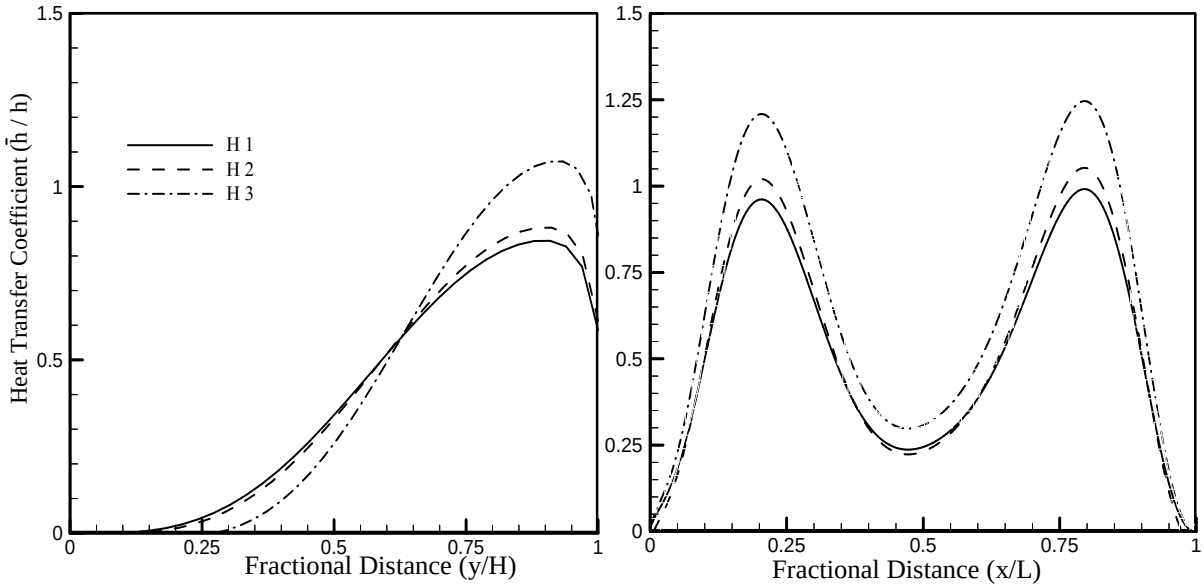

Fig.17: Effect of thermal boundary conditions on the distribution of heat transfer coefficient

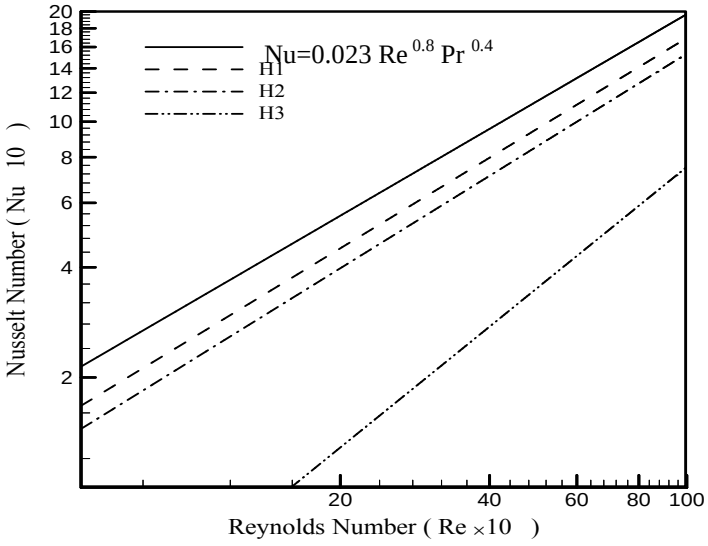

Fig.18: Predicted Nusselt Number in 3-Cusp Duct.